

Xuelong Navigation in Fast Ice Near the Zhongshan Station, Antarctica

AUTHORS

Xianwei Wang

State Key Laboratory of Remote Sensing Science and College of Global Change and Earth System Science, Beijing Normal University, and The Ohio State University

Xiao Cheng

Fengming Hui

State Key Laboratory of Remote Sensing Science and College of Global Change and Earth System Science, Beijing Normal University

Cheng Cheng

College of Global Change and Earth System Science, Beijing Normal University

H.S. Fok

School of Geodesy and Geomatics, Wuhan University

Yan Liu

State Key Laboratory of Remote Sensing Science and College of Global Change and Earth System Science, Beijing Normal University

Background

Introduction to Chinese Antarctic Research Expedition

The Chinese Antarctic Research Expedition (CHINARE) team was established in 1984 (Chen, 2008). Its primary objectives were to conduct various scientific research activities and to provide fundamental support for research, which includes transport-

ABSTRACT

Navigation in polar sea regions requires special attention to the sea ice condition because it is a major barrier for an icebreaker to break the drift ice or fast ice, allowing the vessel to keep moving forward. The advancement of remote sensing imagery provides an effective means to classify and identify various features, including different types of sea ice. Hence, it permits fuel and time saving for the entire voyage, especially when drift ice or fast ice becomes a barrier for the icebreaker. In this study, we exploit the potential usage of high-resolution synthetic aperture radar (SAR) imageries from Radarsat-2 to identify sea ice conditions for precise navigation of China's icebreaker vessel (*Xuelong*) during the 29th Chinese Antarctic Research Expedition in December 2012. Different features on the fast ice were identified from horizontal-transmit and horizontal-receive polarized imagery. The potential usage of SAR imagery for precise navigation was confirmed by an expert witness on the *Xuelong* vessel at that time. The final voyage route has validated our analysis of fast ice and navigation of the *Xuelong* vessel. The predicted regions for unloading locations were also found to be matching well with the actual vessel unloading locations after the final voyage route. Keywords: CHINARE, fast ice, navigation, Radarsat-2, *Xuelong* vessel

ing basic supplies to existing base stations and some exploration tasks. Presently, three existing base stations in Antarctica are operated by China: the Greatwall Station (62°12'59"S, 58°57'52"W, established in February 1985), the Zhongshan Station (69°22'24"S, 76°22'40"E, established in February 1989), and the Kunlun Station (80°25'01"S, 77°06'58"E, established in January 2009) (Chen, 1997; Wang et al., 2013). The most current mission, the 29th CHINARE, started a voyage from Guangzhou, China, to Antarctica on November 5, 2012. The vessel, called *Xuelong*, was installed as an ice breaker, which carried many researchers and equipment and supplies to the Zhongshan Station and the Kunlun Station. This voyage was accomplished on April 9, 2013.

Navigation Challenge in the Prydz Bay

The presence of sea ice in the Prydz Bay represents a great challenge to *Xuelong* navigation between November and December every year. When the temperature drops, ocean water could freeze below the freezing point and form sea ice. Sea ice would be flat and homogeneous when the gradual thickening process does not collide with surrounding ice, rafting, or ridging (Leppäranta, 2011). Otherwise, sea ice with a rough surface or heterogeneous character would occur.

Both drift ice and fast ice are encountered when the *Xuelong* vessel has to cross the Prydz Bay before approaching the Zhongshan Station. Drift ice is the floating sea ice in the ocean primarily driven by wind and/or ocean currents (Armstrong et al., 1966).

Contrary to drift ice, fast ice is the ice anchored to a landmass that remains stationary in place (Leppäranta, 2011). In this bay, the annual maximum ice thickness was about 1.74 m, and its ice growth period was greater than 277 days (Lei et al., 2010). This type of ice is the major barrier for the *Xuelong* vessel to keep moving forward during the voyage, because the icebreaker can only break up the fast ice at a thickness of about 1.2 m (Chen, 1997; Chircop, 2011). In addition to icebreaking, containers with different supplies (e.g., food, fuel, equipment, etc.) have to be unloaded on the fast ice first and then transferred to the Zhongshan Station by snowmobile or helicopter. The fuel being supplied is also required to fill the fuel tanks at the Zhongshan Station through pipelines.

Thus, finding an optimal path for the *Xuelong* vessel during the voyage to the Zhongshan Station is critical to safe and swift navigation across the fast ice zone, in addition to searching for a proper place for unloading different supplies. This paper aims to describe synergetic usage of different data sets (Radarsat-2, Landsat) that could help find the optimal path before navigation in fast ice zones, which has rarely been reported in the recent literature.

Remote Sensing Data Usage and Methodology

Sea ice properties and its spatial coverage in polar regions have been studied for the past two decades. Both optical and microwave remotely sensed data, for example, advanced very-high-resolution radiometer, Landsat, Moderate Resolution Imaging Spectroradiometer Onboard Terra and Auqa (MODIS), Advanced

Microwave Scanning Radiometer-EOS, Envisat, and Radarsat (Arkett et al., 2008; Cavalieri et al., 2006; Kern et al., 2007; Lythe et al., 1999; Ochilov & Clausi, 2012; Ramsay, 1998; Scheuchl et al., 2001; Spreen et al., 2008), have been used to identify sea ice and subsequently used to produce sea ice concentration maps. These sea ice extent and concentration maps are publicly available for scientific or civil usage at <http://www.natice.noaa.gov/ims/>, <http://arctic.atmos.uiuc.edu/cryosphere/>, and <http://www.iup.uni-bremen.de/seaice/amsr/>.

In fact, the spatial coverage variation and fast ice movement in polar regions are of great concern to the scientific community (Giles et al., 2008, 2011; Hirose & Vachon, 1998; Ushio, 2006; Yackel & Barber, 2007). Mahoney et al. (2004, 2007a, 2007b) carried out research on the extent and movement of fast ice in Alaska. A method for retrieving the fast ice extent with high spatio-temporal resolution data was introduced, and fast ice maps in the East Antarctica were generated by Fraser et al. (2010, 2012) with MODIS data. Fast ice evolution over the Resolute Channel, Northwest Territories, Canada, was observed by 1-day interferograms with European remote sensing tandem data from which cracks could be identified clearly (Hirose & Vachon, 1998). Additionally, a system for icebreaker navigation in the Baltic Sea was developed by Berglund et al. (2007). All the above-described works are of utmost importance for expedition planning.

Because of the limitation of optical sensors, data are unavailable when clouds are present. In this paper, we present our results using the high-resolution synthetic aperture radar (SAR) imagery and an associated method for scientific

routing for the navigation and selection of supply unloading locations for China's *Xuelong* vessel in the fast ice region in Antarctic seas.

In order to obtain the fast ice conditions around the *Xuelong* vessel, the necessary data identified for use were at 15:59, November 29, 2012, data from Radarsat-2 C band SAR Georeferenced Fine resolution data with fine mode, dual polarization, and spatial resolution of about 8 m. The data were ordered on November 27, 2012, 2 days before the *Xuelong* approaching this region.

To derive effective information from the imagery, three processing steps have to be done, which include (1) image geocoding, (2) image interpretation, and (3) thematic mapping.

Image Geocoding

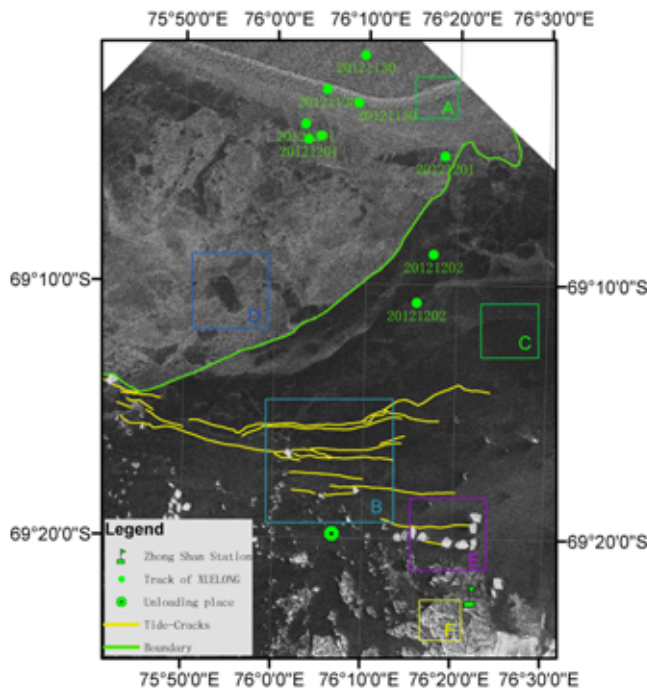
To geocode the imagery, Next European Space Agency SAR Toolbox 4C-1.1 was used. Universal Transverse Mercator (UTM) 43(S) was selected as the projected coordinate system. Because horizontal-transmit and vertical-receive (HV) data may not be useful for classification of new, young, and smooth first-year sea ice (Abreu et al., 2003), the geocoded imagery with horizontal-transmit and horizontal-receive (HH) polarization was selected as the primary data source owing to its better performance on crack identification than the HV data.

Image Interpretation

An ice jam shows a light color with a high digital number (DN) value ("A" in Figure 1) but a wrinkled pattern in the HH polarized imagery. The imagery feature is shown in Figure 2(a). We speculated that the ice jam was formed by refrozen pack ice, which was caused by the collision of neighboring fast ice by strong wind and

FIGURE 1

Radarsat-2 imagery used for *Xuelong* navigation during the 29th CHINARE. At the time of data acquisition, the *Xuelong* vessel did not appear in this imagery. The locations of the *Xuelong* vessel from November 29, 2012 to December 2, 2012 were identified using GPS (green dots). Tide cracks were indicated with yellow polylines. The boundary of smooth fast ice was indicated with green polyline. The ice jam (ridged ice) was indicated with green rectangle "A." Tide cracks were indicated by light blue rectangle marked with "B." Smooth and flat fast ice was indicated by green rectangle marked with "C." The rugged fast ice was indicated by dark blue rectangle marked with "D." Icebergs were indicated by pink rectangle marked with "E." Rocks were indicated by yellow rectangle marked with "F." The final unloading place was marked in a large green circle with one point in the center. UTM-43S was selected as the projected coordinate system in this imagery. (Color versions of figures are available online at: <http://www.ingentaconnect.com/content/mts/mts/2014/00000048/00000001>.)



swell. Because of collision, deformation, overlapping, and refreezing of pack ice, a highly rugged surface was formed. Due to the highly rugged surface and corner reflector effect of overlapping sea ice, the radar signal was largely reflected back as light color shown in the imagery. The overlapping sea ice surface facing to the radar antenna also shows light color. The ice jam always shows linear features and stretches for several miles, which could be clearly seen from SAR imagery.

Tide cracks in fast ice show light color and a linear feature in HH po-

larized imagery ["B" in Figure 1 and Figure 2(b)]. In the fast ice zone, tide cracks are almost parallel to the coastline and are primarily caused by the vertical movement of ocean water due to tides. The sea ice forming the tide cracks always moves up and down with the tide water, and the neighboring ice collides with each other, which results in ridges. Also, sea water running into the surface near the crack can freeze and form ridges [Figures 3(a) and 3(b)]. Because of the corner reflector effect, tide cracks could reflect radar signals ef-

fectively. Additionally, the tide cracks always stretch for several miles in fast ice.

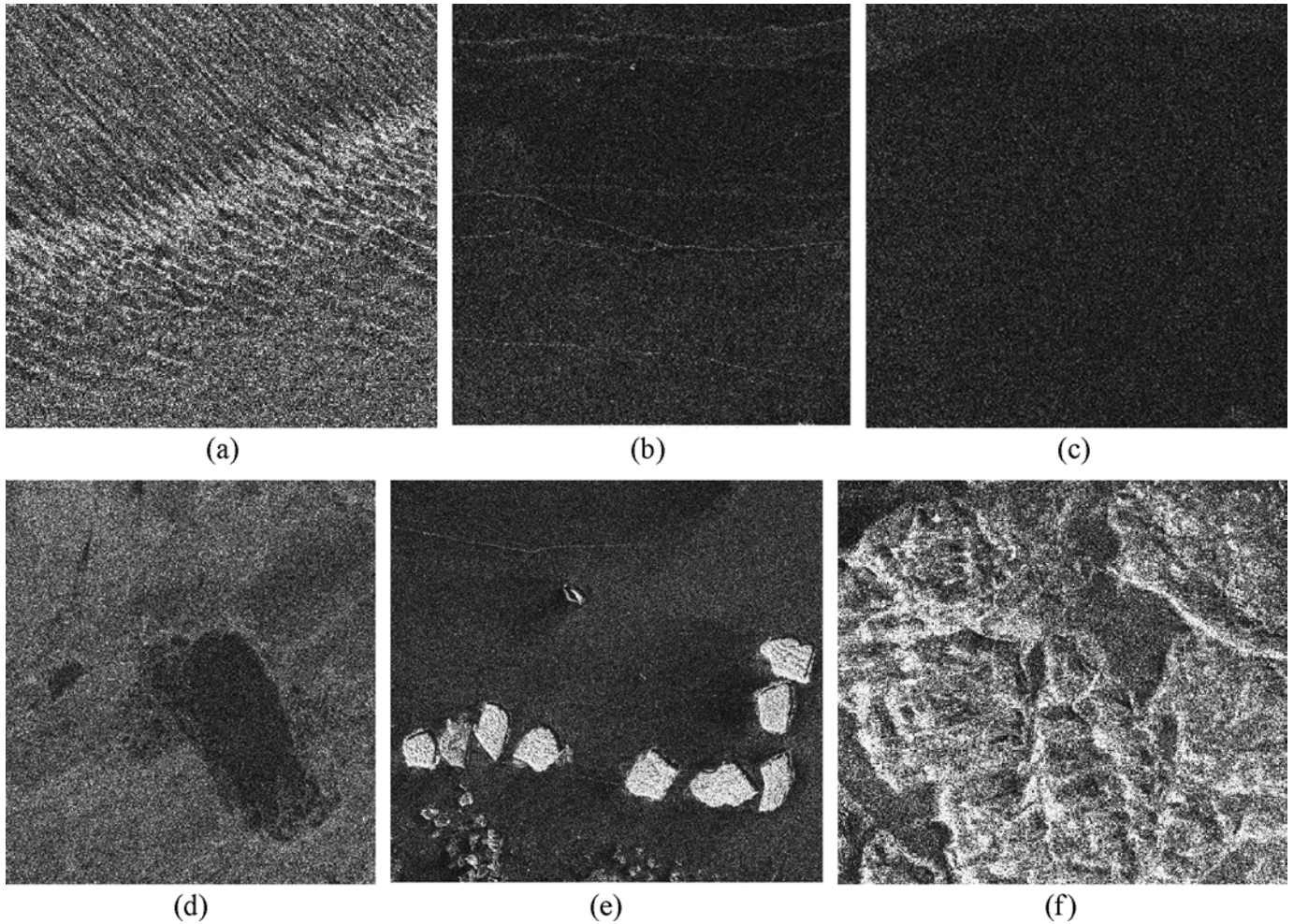
Smooth fast ice shows homogenous dark color in the imagery with low DN values because of the specular reflection of radar wave ["C" in Figure 1 and Figure 2(c)]. Radarsat-2 does not observe from the nadir direction. Thus, fewer radar echoes can be received from those flatter surfaces. Fast ice in this region may be grown from sea water directly, getting thicker gradually. It did not experience breaking into pieces, refreezing, or deformation, resulting in a flat reflected surface. If there is no snow covering the smooth fast ice, the reflected radar signals are primarily from volume scattering. Otherwise, they are from snow layer scattering and volume scattering. It is difficult to tell whether there is snow cover using the SAR imagery only.

Rugged fast ice shows a mixture of both dark and light colors ["D" in Figure 1 and Figure 2(d)], with the dark color indicating fast ice with a smooth surface and the light color indicating the fast ice with a rugged surface or containing deformed or refrozen drift ice. The sea ice in this region may either grow from sea water or be formed by refreezing drift ice. The boundary for flat and rugged fast ice was marked with green polyline in Figure 1.

Icebergs are generated primarily from the disintegration or collapse of ice shelves. Tabular icebergs usually have a vertical edge with spatial extent ranging from several square kilometers to several thousand kilometers for large ones (Martin et al., 2007). The top is always several meters above the sea surface. Thus, a corner reflector is formed. The top surface usually becomes rugged and has many crevasses after icebergs' experiencing melting, wind blowing, and refreezing [Figures 3(c) and 3(d)].

FIGURE 2

Interpretation keys of different features near the Zhongshan Station for Radarsat-2 imagery. (a), (b), (c), (d), (e), and (f) show the typical imagery features about ice jam, tide cracks, flat and homogenous sea ice, rugged fast ice, icebergs, and rocks, respectively.



The iceberg shows a high light color [“E” in Figure 1 and Figure 2(e)] because of the rugged surface and strong corner reflection of radar signals.

Rocks on shore or islands could provide an anchor for fast ice production. The rock surface is always rough. Because of rough terrain and the slant range measurement of the radar sensor, a foreslope always corresponds to strong returns and light features in the imagery, whereas a backslope always corresponds to weak returns and dark features in the imagery (Hanssen, 2001). The color difference of rocks showing in the imagery is primarily

a result of different slopes facing the Radarsat-2 satellite [“F” in Figure 1 and Figure 2(f)].

Thematic Mapping

After interpretation, the thematic map was produced with ArcGIS software. To save satellite communication cost, the thematic map was saved as a JPG file with condensed format and sent to the *Xuelong* vessel on November 30, 2012. To achieve this goal, a proper condensation rate was chosen to balance the capacity of this figure and the imagery details.

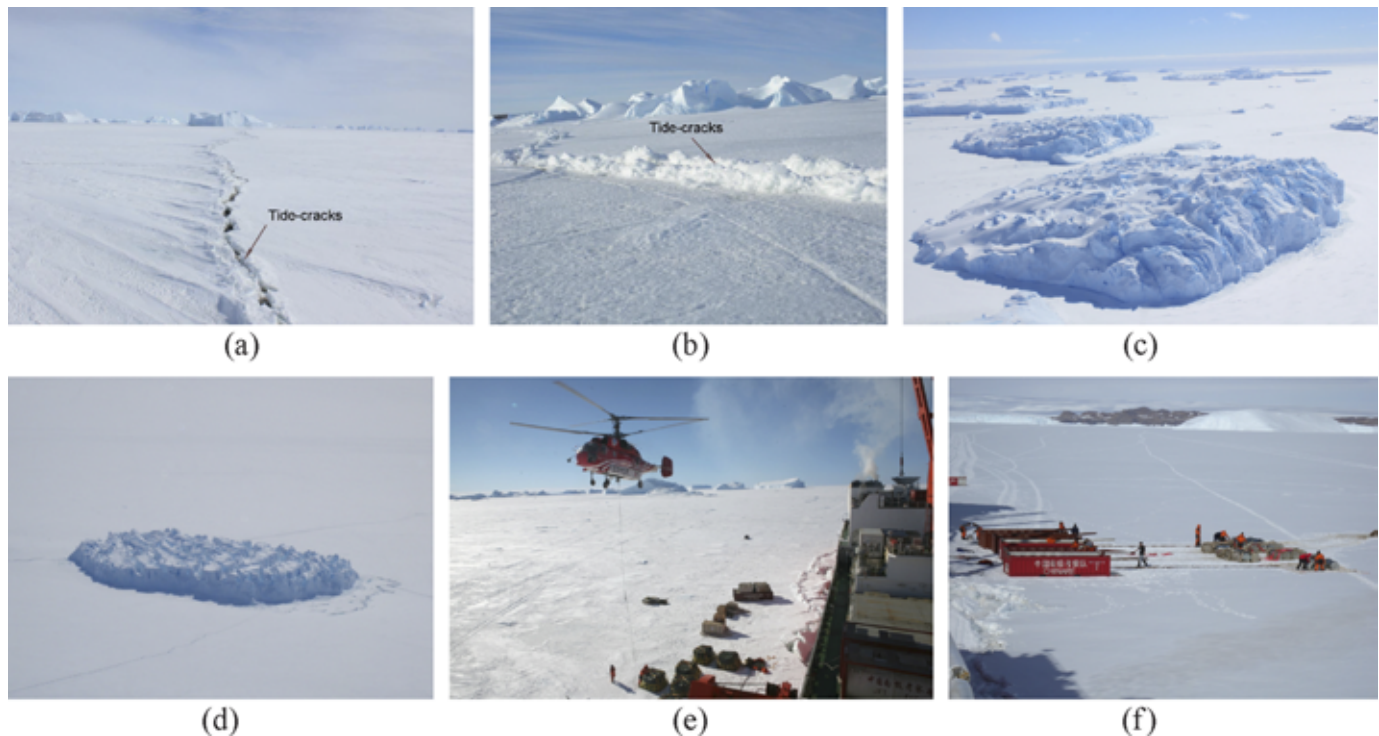
Results and Discussion

Results

Figure 1 shows the thematic map for *Xuelong* navigation in the fast ice of Prydz Bay. From the upper region (northern direction) of this figure, there is an ice jam (disordered ice, ridged ice, and rafted ice, like region “A” in Figure 1) that is about 1-km wide in the southward direction of icebreaking. This is a barrier for *Xuelong* icebreaking because much ice was accumulated and the sea ice may be thicker than that in other places. However, the *Xuelong* has to break it to keep advancing

FIGURE 3

In situ pictures of icebergs, tide cracks, and unloading screen. All the pictures were taken to the north of the Zhongshan Station. (a) and (b) correspond to tide cracks. (c) and (d) correspond to icebergs. (e) and (f) are *in situ* pictures when unloading. (a), (c), and (e) were taken by Dr. Fengming Hui in December 2012 during the 29th CHINARE, and (b), (d), and (f) were taken by Dr. Xianwei Wang in December 2009 during the 26th CHINARE.



southward toward the Zhongshan Station.

There are nine large icebergs ($76^{\circ}13'E-76^{\circ}23'E$, $69^{\circ}19'S-69^{\circ}21'S$) with an area larger than $500\text{ m} \times 500\text{ m}$, distributed in the shape of an L, about 4 km from the Zhongshan Station (see rectangle “E” in Figure 1). The largest distance between two adjacent icebergs is about 1.1 km. This poses another threat for cargo unloading. Because of basal melting/refreezing and the continuous effect of ocean currents and wind to icebergs during austral winter, the icebergs imbedded in the fast ice cannot maintain an equilibrium state. When transferring cargos, the shock from snowmobile traffic may lead to iceberg flipping, which could be disastrous.

In the northwest part, about 8–16 km from the Zhongshan Station,

there are more than nine tide cracks (yellow lines in Figure 1) in the fast ice, which potentially pose a danger for unloading or transferring cargos with snowmobiles. The *Xuelong* vessel will stop icebreaking when it approaches within 10 km of the Zhongshan Station. Thus, this region should not be selected as the unloading site.

The unloading location [Figures 3 (e) and 3(f)] should be selected to be far from icebergs and tide-crack regions. The fast ice at the chosen location must be firm enough to provide a buttress for the working spot because life safety is undoubtedly the most important factor in the Antarctic expedition.

To the northeast of the Zhongshan Station ($76^{\circ}24'E-76^{\circ}30'E$, $69^{\circ}16'S-69^{\circ}22'S$), the fast ice has a smooth surface with fewer tide cracks and fewer

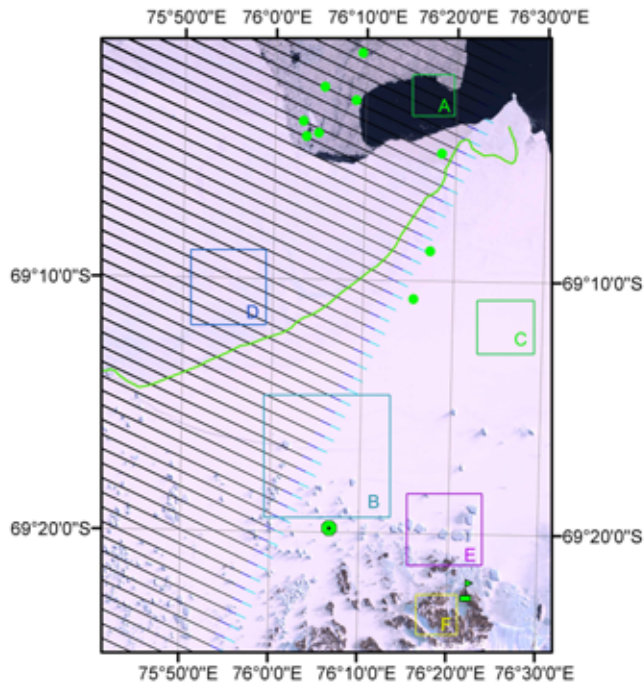
icebergs detected from the imagery, which suggests that this region is a proper place for unloading supplies. However, the sea ice in this flat ice region may be firmer, so that the *Xuelong* vessel cannot be navigated through. Alternatively, to the northwest of the Zhongshan Station, the flat and homogenous fast ice surface ($76^{\circ}9'E-76^{\circ}16'E$, $69^{\circ}17'S-69^{\circ}22'S$) with several nearby islands could also be a proper unloading location. The islands in this region can provide more buttresses for the fast ice that hardens the ice.

Land Cover Identification With Landsat Imagery

Figure 4 shows an optical remotely sensed image (true color imagery comprising bands 3, 2, and 1) from Landsat 7 Enhanced Thematic Mapper Plus (ETM+) acquired on November 22,

FIGURE 4

Landsat 7 ETM+ data captured on November 22, 2012, 7 days before the acquisition of Radarsat-2 imagery (true color image; composed of bands 3, 2, and 1). The data gaps were caused by scan lines corrector failure since May 31, 2003. A, B, C, D, E, and F correspond to the same location indicated in Figure 1. The legend is the same as that in Figure 1.



2013, 7 days earlier than that of Radarsat-2 imagery. Despite different acquisition date between the two images, a comparison could be made between the different features of the same land cover since the change of fast ice should be negligible.

From Figure 4, the fast ice obviously was covered with snow. This cannot be determined from the Radarsat-2 image. The ice jam shown in rectangle “A” of Figure 1 did not occur in that of Figure 4, presumably because the fast ice was formed by refrozen pack ice and was reshaped by strong wind at a later time. Pack ice was pressed together by the strong wind and refrozen, forming the ice jam. On the contrary, not many tide cracks in rectangle “B” of Figure 4 were shown when compared to that of Figure 1. Landsat ETM+ imagery has a resolution of 30 m, making

it unable to observe narrow tide cracks. Only two large tide cracks could be detected there. Land cover in rectangles “C” and “D” did not show much difference between Figures 1 and 4. Based on the comparison, we determined that Landsat 7 ETM+ was not as effective as Radarsat-2 imagery in sea ice discrimination. From rectangles “E” and “F” of Figure 4, one could also clearly identify icebergs and rocks.

Validation

From Figures 1 and 4, we could find that all the interpretations are correct in rectangles “B,” “E,” and “F.” There are no *in situ* data to help validate the flat and rugged fast ice marked in rectangles “C” and “D.” There are also no available data to validate the interpretation of the ice jam marked in rectangle “A.” One could only rely on a per-

son with field experience at that time. Dr. Fengming Hui, who took part in the 29th CHINARE, stated that the above interpretation was correct.

The final route of the *Xuelong* vessel, marked with black arrow, can be seen as a faint southward line in Figure 5. This route validates our result in Section 3. The final route of the vessel was located in the right side of boundary in Figure 5 and did not go deep into the flat fast ice region, where it was suggested. The heavy cracked region marked in rectangle “B” in Figure 1 was crossed safely. Also, when approaching the Zhongshan station, the *Xuelong* vessel did not navigate close to the large icebergs.

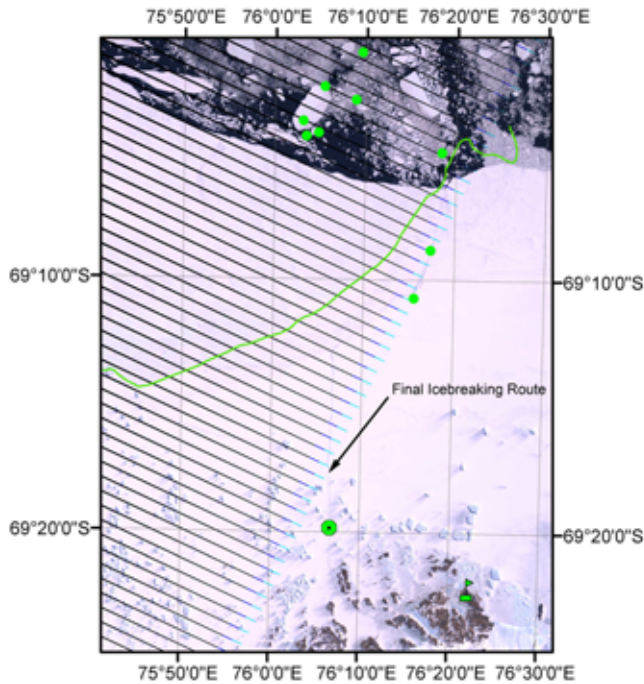
The final unloading place (76°6'E, 69°20'S) marked with a green circle with one point in the center in Figures 1, 4, and 5 was quite near our suggested region to the northwest of the Zhongshan Station (76°9'E-76°16'E, 69°17'S-69°22'S). The linear distance from the unloading place to the Zhongshan Station was about 11 km. In latitude, it almost fell in the center of our predicted region. In longitude, there was a distance of about 3 feet apart geographically, corresponding to about 1.8 km. Our predicted unloading place was much closer to the Zhongshan Station than that. Perhaps, the ice thickness around the tiny region was beyond *Xuelong*'s icebreaking capacity, rendering *Xuelong* unable to move further forward.

Conclusion

Icebreaker navigation for Antarctica research expeditions in a fast ice zone has seldom been reported before because of the limitations of near-real-time satellite observation and the difficulty in interpretation based on those satellite data. Traditionally, expedition members get off the icebreaker

FIGURE 5

Landsat 7 ETM+ data captured on December 29, 2012 (true color image; composed of bands 3, 2, and 1). The data gaps were caused by scan lines corrector failure since May 31, 2003. The legend is the same as that in Figure 1.



and detect the sea ice on snowmobiles when the vessel is icebreaking. This is quite dangerous. There may be cracks anywhere in the fast ice covered by snow, which cannot easily identified by human eyes, not to mention the regions with smooth or rugged fast ice even with limited ice drilling holes.

In this research, image interpretation and field work experience are indispensable to identify different features from Radarsat-2 imagery. Compared with Landsat-7 ETM+ data, our analysis is confirmed. This is just one case of polar navigation in the fast ice region. An automatic method should be further developed to fulfill the automatic navigation in the near future.

After the launch of additional SAR satellites, such as Radarsat-2, Constellation of Small Satellites for the Medi-

terranean Basin Observation-SkyMed, and TerraSAR-X, the imageries with high resolution at a level of several meters can be utilized for icebreaker navigation in fast ice zone or drift ice near the Antarctica. For *Xuelong* navigation in fast ice, high-resolution SAR data are the best choice because it can penetrate clouds and give a detailed screening of the local sea ice. For CHINARE, it is particularly important to use the near real-time and high-resolution SAR data for icebreaking route selection and cargo unloading place selection because no other effective sensor was equipped on the *Xuelong* vessel to obtain sea ice conditions. It is, therefore, highly recommended that a combination of full polarization data be used for polar navigation in the near future in order to identify different types of sea ice in a timely and efficient manner.

Acknowledgments

We are grateful to the support from the Chinese Arctic and Antarctic Administration. This research is partially supported by China Postdoctoral Science Foundation (grant nos. 2012M520185 and 2013T60077), National Natural Science Foundation of China (Grant nos. 41106157, 41176163, and 41374010), and China Research Foundation on Polar Science and National High Technology Research and Development Program of China (grant no. 2008AA121702). We are grateful to two anonymous reviewers and Prof. C. K. Shum for their constructive comments, which have led to substantial improvement of this paper.

Corresponding Authors:

Xianwei Wang, State Key Laboratory of Remote Sensing Science, Beijing Normal University, and The Ohio State University
Email: wangxianwei0304@163.com
Xiao Cheng, State Key Laboratory of Remote Sensing Science and Beijing Normal University
Email: xcheng@bnu.edu.cn

References

- Abreu, R.D., Flett, D., Scheduchl, B., & Ramsay, B. 2003. Operational sea ice monitoring with RADARSAT-2—A glimpse into the future. *Int Geosci Remote Se.* 2:1308-10.
- Arkett, M., Flett, D., Abreu, R.D., Clemente-Colon, P., Woods, J., & Melchior, B. 2008. Evaluating ALOS-PALSAR for ice monitoring—What can L-band do for the North American Ice Service? *Int Geosci Remote Se.* 5:188-191.
- Armstrong, T., Roberts, B., & Swithinbank, C. 1966. *Illustrated Glossary of Snow and Ice.* Cambridge, UK: Scott Polar Research Institute.
- Berglund, R., Kotovirta, V., & Seina, A. 2007. A system for icebreaker navigation and assistance planning using spaceborne SAR

- information in the Baltic Sea. *Can J Remote Sens.* 33(5):378-387. <http://dx.doi.org/10.5589/m07-042>.
- Cavaliere**, D., Markus, T., Hall, D., Gasiewski, A., Klein, M., & Ivanoff, A. 2006. Assessment of EOS Aqua AMSR-E Arctic sea ice concentrations using Airborne Microwave and Landsat 7 imagery. *IEEE T Geosci Remote.* 44(11):3057-69. <http://dx.doi.org/10.1109/TGRS.2006.878445>.
- Chen**, L. 1997. Review of Chinese Antarctic research expeditions. *Adv Earth Sci.* 12(2):127-33.
- Chen**, L. 2008. A review and perspective on Chinese Arctic and Antarctic research expedition. *Bull Nation Nat Sci Found China.* 22(4):199-203.
- Chircop**, A. 2011. The emergence of China as a polar-cable state. *Can Naval Rev.* 7(1):9-14.
- Fraser**, A.D., Massom, R.A., & Michael, K.J. 2010. Generation of high-resolution East Antarctic landfast sea-ice maps from cloud-free MODIS satellite composite imagery. *Remote Sens Environ.* 114(12):2888-96. <http://dx.doi.org/10.1016/j.rse.2010.07.006>.
- Fraser**, A.D., Massom, R.A., Michael, K.J., Galton-Fenzi, B.K., & Lieser, J.L. 2012. East Antarctic landfast sea ice distribution and variability, 2000-2008. *J Climate.* 25(4):1137-56. <http://dx.doi.org/10.1175/JCLI-D-10-05032.1>.
- Giles**, A.B., Massom, R.A., Heil, P., & Hyland, G. 2011. Semi-automated feature-tracking of East Antarctic fast ice and pack ice from Envisat ASAR imagery. *Remote Sens Environ.* 115:2267-76. <http://dx.doi.org/10.1016/j.rse.2011.04.027>.
- Giles**, A.B., Massom, R.A., & Lytle, V.I. 2008. Fast ice distribution in East Antarctica during 1997 and 1999 determined using Radarsat data. *J Geophys Res.* 113:C02S14. <http://dx.doi.org/10.1029/2007JC004139>.
- Hanssen**, R.F. 2001. *Radar Interferometry: Data Interpretation and Error Analysis.* Dordrecht, Netherlands: Kluwer Academic Publishers.
- Hirose**, T., & Vachon, P.W. 1998. Demonstration of ERS tandem mission SAR interferometry for mapping Land Fast Ice Evolution. *Can J Remote Sens.* 24(1):89-92.
- Kern**, S., Spreen, G., Kaleschke, L., de La Rosa, S., & Heygster, G. 2007. Polynya Signature Simulation Method polynya area in comparison to AMSR-E 89 GHz sea ice concentrations in the Ross Sea and off the Adélie Coast, Antarctica, for 2002-05: First results. *Ann Glaciol.* 46:409-18. <http://dx.doi.org/10.3189/172756407782871585>.
- Lei**, R., Li, Z., Cheng, B., Zhang, Z., & Heil, P. 2010. Annual cycle of landfast sea ice in Prydz Bay, east Antarctica. *J Geophys Res.* 115:C02006. <http://dx.doi.org/10.1029/2008JC005223>.
- Leppäranta**, M. 2011. *The Drift of Sea Ice.* Berlin, Germany: Springer-Verlag. ISBN 978-3-642-04682-7. <http://dx.doi.org/10.1007/978-3-642-04683-4>.
- Lythe**, M., Hauser, A., & Wendler, G. 1999. Classification of sea ice types in the Ross Sea, Antarctica from SAR and AVHRR imagery. *Int J Remote Sens.* 20(15):3073-85. <http://dx.doi.org/10.1080/014311699211624>.
- Mahoney**, A., Eicken, H., Gaylord, A.G., & Shapiro, L. 2007a. Alaska landfast sea ice: Links with bathymetry and atmospheric circulation. *J Geophys Res.* 112:2001. <http://dx.doi.org/10.1029/2006JC003559>.
- Mahoney**, A., Eicken, H., Graves, A., Shapiro, L., & Cotter, P. 2004. Landfast sea ice extent and variability in the Alaskan Arctic derived from SAR imagery. *Int Geosci Remote Se.* 3:2146-9.
- Mahoney**, A., Eicken, H., & Shapiro, L. 2007b. How fast is landfast sea ice? A study of the attachment and detachment of near-shore ice at Barrow, Alaska. *Cold Reg Sci Technol.* 47:233-55. <http://dx.doi.org/10.1016/j.coldregions.2006.09.005>.
- Martin**, S., Drucker, R.S., & Kwok, R. 2007. The areas and ice production of the western and central Ross Sea polynyas, 1992-2002, and their relation to the B-15 and C-19 iceberg events of 2000 and 2002. *J Marine Syst.* 68(1-2):201-14. <http://dx.doi.org/10.1016/j.jmarsys.2006.11.008>.
- Ochilov**, S., & Clausi, D.A. 2012. Operational SAR sea-ice image classification. *IEEE T Geosci Remote.* 50(11):4397-408. <http://dx.doi.org/10.1109/TGRS.2012.2192278>.
- Ramsay**, B.H. 1998. The interactive multi-sensor snow and ice mapping system. *Hydrol Process.* 12:1537-46. [http://dx.doi.org/10.1002/\(SICI\)1099-1085\(199808/09\)12:10/11<1537::AID-HYP679>3.0.CO;2-A](http://dx.doi.org/10.1002/(SICI)1099-1085(199808/09)12:10/11<1537::AID-HYP679>3.0.CO;2-A).
- Scheuchl**, B., Caves, R., Cumming, I., & Staples, G. 2001. Automated sea ice classification using spaceborne polarimetric SAR data. *Int Geosci Remote Se.* 7:3117-9.
- Spreen**, G., Kaleschke, L., & Heygster, G. 2008. Sea ice remote sensing using AMSR-E 89 GHz channels. *J Geophys Res.* 113:C02S03. doi: 10.1029/2005JC003384.
- Ushio**, S. 2006. Factors affecting fast-ice break-up frequency in Lützw-Holm Bay, Antarctica. *Ann Glaciol.* 44:177-82. <http://dx.doi.org/10.3189/172756406781811835>.
- Wang**, X.W., Cheng, X., Huang, H.B., & Li, Z. 2013. DEM generation in Dome-A area with GLAS and GPS data. *J Remote Sens.* 17(2):424-9.
- Yackel**, J.J., & Barber, D.G. 2007. Observations of snow water equivalent change on landfast first-year sea ice in winter using synthetic aperture radar data. *IEEE T Geosci Remote.* 45:1005-15. <http://dx.doi.org/10.1109/TGRS.2006.890418>.